

# ABS-Mamba: SAM2-Driven Bidirectional Spiral Mamba Network for Medical Image Translation

Feng Yuan<sup>1,2</sup>, Yifan Gao<sup>1,3</sup>, Wenbin Wu<sup>1,2</sup>, Keqing Wu<sup>1,2</sup>, Xiaotong Guo<sup>1,2</sup>, Jie Jiang<sup>1,2</sup>, Xin Gao<sup>2</sup>

<sup>1</sup> School of Biomedical Engineering (Suzhou), Division of Life Science and Medicine, University of Science and Technology of China, Hefei, China<sup>1</sup>

<sup>2</sup> Suzhou Institute of Biomedical Engineering and Technology, Chinese Academy of Sciences, Suzhou, China<sup>2</sup>

<sup>3</sup> Shanghai Innovation Institute, Shanghai, China<sup>3</sup>

yuanfeng2317@mail.ustc.edu.cn, yifangao@mail.ustc.edu.cn,

wenbinwu@mail.ustc.edu.cn, keqingw@mail.ustc.edu.cn,

gxt13780405276@163.com, jiejiang-ustc@mail.ustc.edu.cn, xingaosam@163.com

**Abstract.** Accurate multi-modal medical image translation requires harmonizing global anatomical semantics and local structural fidelity, a challenge complicated by intermodality information loss and structural distortion. We propose ABS-Mamba, a novel architecture integrating the Segment Anything Model 2 (SAM2) for organ-aware semantic representation, specialized convolutional neural networks (CNNs) for preserving modality-specific edge and texture details, and Mamba’s selective state-space modeling for efficient long- and short-range feature dependencies. Structurally, our dual-resolution framework leverages SAM2’s image encoder to capture organ-scale semantics from high-resolution inputs, while a parallel CNNs branch extracts fine-grained local features. The Robust Feature Fusion Network (RFFN) integrates these representations, and the Bidirectional Mamba Residual Network (BMRN) models spatial dependencies using spiral scanning and bidirectional state-space dynamics. A three-stage skip fusion decoder enhances edge and texture fidelity. We employ Efficient Low-Rank Adaptation (LoRA+) fine-tuning to enable precise domain specialization while maintaining the foundational capabilities of the pre-trained components. Extensive experimental validation on the SynthRAD2023 and BraTS2019 datasets demonstrates that ABS-Mamba outperforms state-of-the-art methods, delivering high-fidelity cross-modal synthesis that preserves anatomical semantics and structural details to enhance diagnostic accuracy in clinical applications. The code is available at <https://github.com/gatina-yone/ABS-Mamba>.

**Keywords:** Medical Image Translation · SAM2 · Mamba · LoRA+

## 1 Introduction

Multi-modal medical images provide complementary diagnostic information through distinct tissue contrast mechanisms, widely utilized in clinical workflows

for disease screening and treatment planning [1, 2]. These modality-specific contrasts deliver critical anatomical information and enhance the accuracy of computational analyses [3]. However, acquiring complete multi-modal datasets is challenging due to time constraints, image corruption, and diverse imaging protocols, restricting their routine clinical adoption [4–6]. This drives the development of computational medical image translation frameworks, which offer objective, reproducible outcomes to support clinical decision-making and personalized medicine [7, 8].

Anatomical tissues display complex, spatially varying distributions, often forming intricate clusters [9]. This complexity demands the extraction of fine-grained local features and global dependencies in multi-modal medical image translation. In recent years, Generative Adversarial Networks (GANs) have excelled in preserving textures during cross-modal synthesis, yet they frequently fail to ensure global anatomical coherence in high-resolution imaging [10]. Conversely, Vision Transformers (ViTs) adeptly capture long-range dependencies, but their quadratic computational complexity restricts efficiency for high resolution medical datasets [11].

Recent advances in state space models, such as Mamba, efficiently model pixel sequences by utilizing state-space operators to capture both long- and short-range contextual dependencies [12–17]. These models leverage differential equations to enhance the representation of complex interactions between texture and anatomical structures in medical images. Concurrently, vision foundation models like SAM and SAM2 demonstrate promising generalization and few-shot adaptability across diverse visual tasks [18–20]. SAM2, in particular, features architectural improvements and has been trained on an extensive dataset of over 1 million images and 50,000 videos, including more than 1.1 billion semantic masks. Combining the efficient long-range contextual modeling of state space models with the advanced semantic understanding of SAM2 opens up new possibilities for solving the challenges in accurate medical image translation.

In this work, we present ABS-Mamba, a novel image translation network designed to capture global contextual semantics and detailed features for accurately generating target domain images. Its key innovation stems from a unique integration strategy that combines SAM2’s image encoder for global semantic modeling, a CNNs-based encoder for local feature extraction, and Mamba’s efficient bidirectional serialized interaction to optimize cross-modal feature complementarity and computational efficiency. The proposed network adopts a U-shaped architecture comprising three core components: encoder, backbone, and decoder. 1) The hybrid encoder combines SAM2’s pretrained Hiera image encoder, which captures hierarchical global context, with a specialized CNNs-based domain-specific feature extractor, fusing their outputs via RFFN. 2) The backbone, BMRN, employs channel-wise mixed Mamba modules to facilitate bidirectional interaction, enabling spatially contextual learning across feature maps through a helical scanning trajectory for balanced contextual sensitivity. 3) The decoder preserves low-level spatial features through multi-scale skip connections between corresponding encoder-decoder levels, ensuring retention of anatomical details

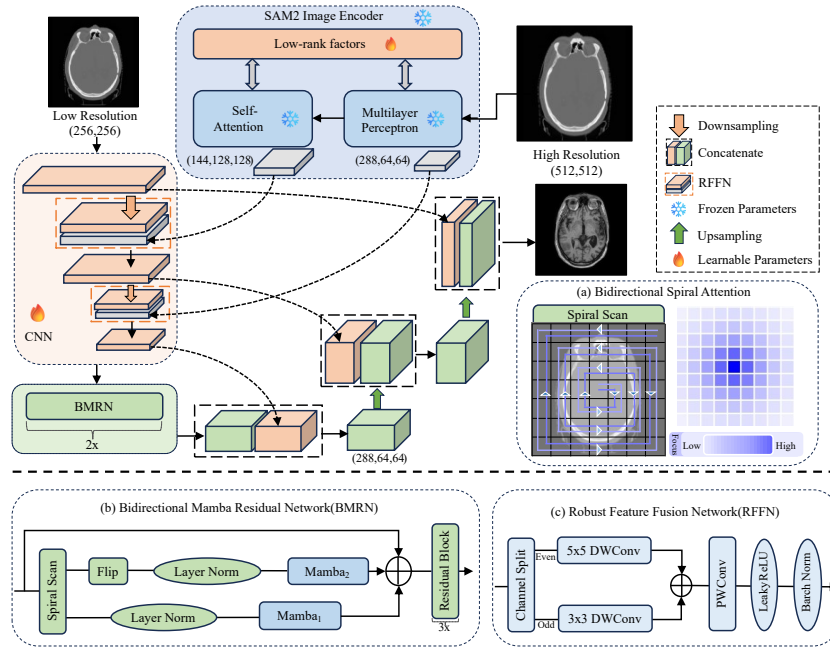


**Fig. 1.** The architecture of ABS-Mamba. The network comprises three key components: (1) a hybrid encoder module that integrates global features from SAM2’s image encoder with local features from convolutional layers through (c) Robust Feature Fusion Network (RFFN); (2) a backbone network utilizing (b) BMRN with bidirectional channel mixing Mamba blocks, which enables efficient short-range and long-range dependency modeling through (a) spiral-scanning trajectories on spatial feature mappings; (3) a multi-level skip-connected decoder that progressively projects contextualized representations onto the target image domain via convolutional upsampling layers.

in clinical-grade image translation by residual concatenation of high-frequency components derived from the encoder.

We extensively evaluate ABS-Mamba on two public datasets: one comprising CT and MRI images of the brain and pelvis, and another consisting of T1- and T2-weighted MRI sequences of the brain. Quantitative results demonstrate that ABS-Mamba outperforms state-of-the-art approaches in synthesizing target-domain images and shows robust generalization across multi-institutional clinical settings.

## 2 Methodology

### 2.1 Overview of ABS-Mamba

ABS-Mamba is a novel architecture that synergistically integrates SAM2’s vision transformer with CNNs-based local feature extractors, enhanced by the recent

Mamba module for longitudinal context modeling. As illustrated in Fig. 1, the hybrid encoder employs a frozen SAM2 image encoder with  $16 \times 16$  patch embedding to process input image with high-resolution of  $512 \times 512$ , while the CNNs branch extracts hierarchical features from images with low-resolution of  $256 \times 256$ . The RFFN dynamically fuses multi-scale features, enabling the model to learn a unified representation that harmonizes complementary information from dual-resolution medical imaging protocols. During training, we adapt Low-Rank Adaptation (LoRA+) on only 19.47% of SAM2’s decoder parameters, maintaining the pretrained model’s diagnostic generalization and enabling domain-specific refinement [22].

The backbone architecture integrates bidirectional channel-mixing Mamba modules to effectively capture long-range contextual dependencies in medical image sequences while maintaining high local fidelity, addressing the inherent noncausal nature of medical imaging data. The BMRN block employs a spiral scanning trajectory to model isotropic spatial context across feature maps, coupled with adaptive channel-mixing layers that hierarchically aggregate cross-channel contextual information, specifically designed for anatomical consistency in medical image translation.

The decoder of ABS-Mamba achieves high-fidelity medical image translation through a three-stage process. During decoding, it hierarchically integrates encoder features via skip connections, incorporating two hybrid confused feature layers and one CNN feature layer.

## 2.2 Hybrid encoder

The hybrid encoder is designed Cross-Resolution Hierarchical Feature Fusion with two parallel pathways: 1) a CNNs encoder processing low-resolution inputs  $X_a \in \mathbb{R}^{256 \times 256}$ . 2) a pre-trained SAM2-Hiera image encoder handling high-resolution inputs  $X_b \in \mathbb{R}^{512 \times 512}$ , which collectively extract multi-scale global contextual features. Cross-modality feature fusion is achieved by RFFN, which applies channel-wise attention mechanisms to align and integrate heterogeneous feature representations from both pathways, ensuring robust multi-scale feature aggregation for downstream tasks.

**Robust Feature Fusion Network(RFFN)** : As illustrated in Fig. 1c, we design a multi-scale depth-wise separable convolutional architecture based on an interleaved splitting strategy, achieving efficient feature fusion through feature channel recombination and multi-kernel parallel processing. The feature tensor output from the  $i$ -th layer of the hybrid encoder is defined as  $F_i \in \mathbb{R}^{C_{in} \times H \times W}$ , where  $C_{in}$  denotes the input channel dimension. First, using the modulo-2 remainder criterion, the input features are decoupled along the channel dimension into two complementary subspaces:

$$\begin{cases} F_{\text{even}} = F_l[:, 2k :: 2, :, :] \\ F_{\text{odd}} = F_l[:, 2k + 1 :: 2, :, :] \end{cases} \quad \forall k \in \{0, 1, \dots, \lfloor C_{in}/2 \rfloor - 1\} \quad (1)$$

where  $F_{even}, F_{odd} \in \mathbb{R}^{B \times (C_{in}/2) \times H \times W}$ . Guided by the feature pyramid theory, convolutional kernels of differing scales ( $3 \times 3$  and  $5 \times 5$ ) are implemented through depth-wise separable convolutions on the decoupled subfeatures respectively, enhancing cross-scale feature completeness [23]. After multi-kernel processing, the decomposed features undergo:

$$\mathbf{F}_{out} = \text{LReLU}\left(\underbrace{\text{BN}(\mathcal{W}_{pw}(Y_s \oplus Y_t))}_{\phi: \mathbb{R}^{C_{in}/2 \times H \times W} \times \mathbb{R}^{C_{in}/2 \times H \times W} \rightarrow \mathbb{R}^{C_{in} \times H \times W}}; \alpha = 0.05\right) \quad (2)$$

where  $\alpha = 0.05$  governs the negative signal retention ratio, enhancing robustness against adversarial samples.  $\mathcal{W}_{pw}$  denotes the  $1 \times 1$  pointwise convolution.

**Cross-Resolution Hierarchical Feature Fusion** : Let  $f_i^a \in \mathbb{R}^{C_i \times H_i \times W_i}$  represent the output feature from the  $i$ -th layer of CNNs Encoder. The SAM2-Hiera encoder outputs four hierarchical  $f_j^b \in \mathbb{R}^{C_j \times H_j \times W_j}$ . Where  $C_i, C_j \in \{144, 288, 576, 1152\}$  [24]. Let  $f_{ij}^{ab}$  denotes the fused feature between the  $i$ -th and  $j$ -th layers via RFFN( $f_i^a, f_j^b$ ).

The first layer of the encoder processes single-channel input  $X_a \in \mathbb{R}^{1 \times 256 \times 256}$ , preserving resolution while expanding the channel dimension to 3. Reflection padding(`nn.ReflectionPad2d(3)`) extends it to  $262 \times 262$ , mirroring boundaries to reduce artifacts. A  $7 \times 7$  convolution (a stride of 2) outputs a  $3 \times 256 \times 256$  feature map, followed by BatchNorm and ReLU, yielding  $f_1^a \in \mathbb{R}^{3 \times 256 \times 256}$ . For the second layer, a  $3 \times 3$  convolution with stride=2 downsamples  $f_1^a$  to  $f_2^a \in \mathbb{R}^{144 \times 128 \times 128}$ . After normalization and activation procedures, the RFFN integrates  $f_2^a$  and  $f_1^b$  via residual connections, generating the fused feature  $f_{21}^{ab} \in \mathbb{R}^{144 \times 128 \times 128}$ . The third layer follows this paradigm, further downsampling to  $f_3^{ab} \in \mathbb{R}^{288 \times 64 \times 64}$  and performing secondary fusion with  $f_2^b$ , ultimately producing  $f_{32}^{ab} \in \mathbb{R}^{288 \times 64 \times 64}$ .

### 2.3 Bidirectional Mamba Residual Network

Our proposed BMRN is shown in Fig. 1b, which deploys a spiral scanning mechanism to transform 2D feature representations into progressive spiral sequences. Formally, given an input batch  $X \in \mathbb{R}^{B \times C \times H \times W}$ , the module first applies dimensional reshaping to generate normalized features  $\hat{X}$ . Through predetermined spiral transformation matrices  $S \in \mathbb{R}^{B \times N \times L}$ , executes spatial mapping to get  $\tilde{X}$ :

$$\begin{cases} \hat{X}_1 = \text{Reshape}(X) \in \mathbb{R}^{B \times C \times L} \\ \tilde{X}_1 = S \cdot \hat{X}_1^\top \in \mathbb{R}^{B \times L \times C} \end{cases} \quad L = H \times W \quad (3)$$

As illustrated in Fig. 1a, the bidirectional helical trajectory design effectively captures long-range contextual information. The footprint illustrates the spatial distribution of focus points deployed by each learning operator while seeking contextual interactions for central pixels. For the forward and reverse scanned sequences, we employ separate Mamba for feature extraction. The input tensors

$\tilde{X}_1$  and  $\text{Flip}(\tilde{X}_1, \text{dim} = 1)$  (denoted as  $\tilde{X}_2$ ) undergo Layer Normalization before being fed into two independent state space modules Mamba<sub>1</sub> and Mamba<sub>2</sub>, respectively:

$$\begin{cases} Y_1 = \text{Mamba}_1(\text{LN}(\tilde{X}_1)) \\ Y_2 = \text{Mamba}_2(\text{LN}(\tilde{X}_2)) \end{cases} \quad \text{Mamba}(Z) = \sigma(W_{\text{conv}} * Z) \odot (W_{\text{proj}} \cdot \text{SSM}(Z)) \quad (4)$$

where  $\sigma$  and  $\odot$  denotes Leaky ReLU activation and element-wise multiplication. After concatenating the two-path features, feature fusion is performed using a residual convolutional module:

$$Y = \underbrace{\text{Conv}_{1 \times 1}[X, \text{Conv}_{1 \times 1}[\hat{Y}_1, \hat{Y}_2]] + \mathcal{F}(\text{Conv}_{1 \times 1}[X, \text{Conv}_{1 \times 1}[\hat{Y}_1, \hat{Y}_2]])}_{\phi: \mathbb{R}^{B \times C \times H \times W} \times \mathbb{R}^{B \times C \times H \times W} \times \mathbb{R}^{CB \times C \times H \times W} \rightarrow \mathbb{R}^{B \times C \times H \times W}} \quad (5)$$

where  $\mathcal{F}(\cdot)$  is defined as two consecutive 3x3 convolutional layers, each followed by ReLU activation and batch normalization (BN).

## 3 Experiments and Results

### 3.1 Datasets and Implementation Details

To validate the effectiveness and performance of the proposed ABS-Mamba in medical image translation tasks using the SynthRAD2023 Grand Challenge dataset [25] and BraTS 2019 public dataset [26]. The experiments specifically address two key challenges: metal artifact suppression in brain and pelvic CT to MRI translation, and pulse sequence parameter mapping between T1 and T2 weighted images. The datasets are randomly divided by patient ID into 70% training and 30% testing sets, with SynthRAD data employing axial slice-level stratified sampling and BraTS 2019 following the official partition strategy [26].

We compare ABS-Mamba against several state-of-the-art methods including ResViT [27], VMamba [28], TransUNet [29], DiffMa [30], I2I-Mamba [31], and U-Mamba [32]. Two established metrics are employed for performance assessment: Structural Similarity Index (SSIM) and Peak Signal-to-Noise Ratio (PSNR). All models are trained for 200 epochs on NVIDIA RTX 4090 GPUs with 24GB of memory. The batch size is set to 4. The optimization process utilized Adam optimizer ( $\beta_1 = 0.5, \beta_2 = 0.999$ ) with base learning rate  $2e-4$  and cosine annealing scheduling decaying to  $1e-7$ . The hybrid loss combined adversarial loss ( $\lambda_{adv} = 1$ ) and pixel-level L1 loss ( $\lambda_{pix} = 100$ ). The LoRA+ adaptation layers ( $r = 16, \alpha = 32$ ) are integrated into the SAM2Encoder module, achieving 19.47% trainable parameters of the total architecture with an adapter parameter ratio of  $3.2e-3$ .

### 3.2 Results

To evaluate ABS-Mamba’s performance in CT-to-MRI image translation against state-of-the-art methods using the SynthRAD2023 Grand Challenge dataset (brain and pelvis). The comprehensive benchmarking results in Table 1 demonstrate that ABS-Mamba outperforms existing methods across multiple metrics.

**Table 1.** Quantitative comparison of CT to MRI conversion task on Brain and Pelvis against other baseline methods. PSNR (dB) and SSIM are listed as mean $\pm$ std across the test set. The best results are highlighted in bold.

Methods	Brain		Pelvis	
	SSIM	PSNR	SSIM	PSNR
<b>Dataset: SynthRAD2023 Grand Challenge dataset</b>				
ResViT <sub>(TMI'22)</sub>	0.785 $\pm$ 0.012	21.58 $\pm$ 0.85	0.684 $\pm$ 0.022	24.65 $\pm$ 1.01
TransUNet <sub>(MIA'24)</sub>	0.842 $\pm$ 0.011	24.47 $\pm$ 0.79	0.728 $\pm$ 0.024	26.32 $\pm$ 0.99
U-Mamba <sub>(arXiv'24)</sub>	0.855 $\pm$ 0.015	25.12 $\pm$ 1.02	0.733 $\pm$ 0.019	26.70 $\pm$ 0.88
VMamba <sub>(ICML'24)</sub>	0.859 $\pm$ 0.014	25.23 $\pm$ 1.01	0.736 $\pm$ 0.022	26.49 $\pm$ 0.97
DiffMa <sub>(arXiv'24)</sub>	0.866 $\pm$ 0.009	25.84 $\pm$ 0.88	0.743 $\pm$ 0.012	27.07 $\pm$ 1.01
I2I-Mamba <sub>(arXiv'24)</sub>	<u>0.881<math>\pm</math>0.012</u>	<u>27.69<math>\pm</math>1.01</u>	<b>0.772<math>\pm</math>0.014</b>	<u>27.32<math>\pm</math>1.21</u>
ABS-Mamba <sub>(ours)</sub>	<b>0.896<math>\pm</math>0.015</b>	<b>28.32<math>\pm</math>1.03</b>	<u>0.766<math>\pm</math>0.021</u>	<b>27.78<math>\pm</math>0.79</b>

**Table 2.** Quantitative comparison of T1 to T2 conversion task on Brain against other baseline methods. PSNR (dB) and SSIM are listed as mean $\pm$ std across the test set. The best results are highlighted in bold.

Methods	SSIM	PSNR
<b>Dataset: BraTS 2019 dataset</b>		
ResViT <sub>(TMI'22)</sub>	0.865 $\pm$ 0.013	24.58 $\pm$ 0.75
TransUNet <sub>(MIA'24)</sub>	0.882 $\pm$ 0.012	26.97 $\pm$ 0.69
VMamba <sub>(ICML'24)</sub>	0.903 $\pm$ 0.008	28.42 $\pm$ 0.72
U-Mamba <sub>(arXiv'24)</sub>	0.912 $\pm$ 0.011	29.63 $\pm$ 0.81
DiffMa <sub>(arXiv'24)</sub>	0.915 $\pm$ 0.006	29.76 $\pm$ 0.78
I2I-Mamba <sub>(arXiv'24)</sub>	<u>0.929<math>\pm</math>0.011</u>	<u>30.47<math>\pm</math>0.51</u>
ABS-Mamba <sub>(ours)</sub>	<b>0.935<math>\pm</math>0.009</b>	<b>31.70<math>\pm</math>0.56</b>

It achieves the highest SSIM and PSNR on the brain dataset and the highest PSNR on the pelvis dataset. The difference in SSIM on the pelvis dataset compared to the suboptimal approach is minimal, demonstrating ABS-Mamba’s overall superiority.

We further validate ABS-Mamba on the BraTS 2019 dataset to assess image translation quality. The quantitative results are presented in Table 2, ABS-Mamba achieves an SSIM of 0.935 $\pm$ 0.009 and a PSNR of 31.70 $\pm$ 0.56 dB, outperforming the suboptimal approach by 0.65% in SSIM and 4.03% in PSNR. These results demonstrate the effectiveness of ABS-Mamba in handling handling variations across different clinical sites and scanners.

Fig. 2 presents the visual comparisons of image translation results obtained by different methods for representative examples from the SynthRAD2023 Grand Challenge dataset and BraTS 2019 dataset. These qualitative comparisons highlight the superior performance of ABS-Mamba in achieving accurate translation outcomes.

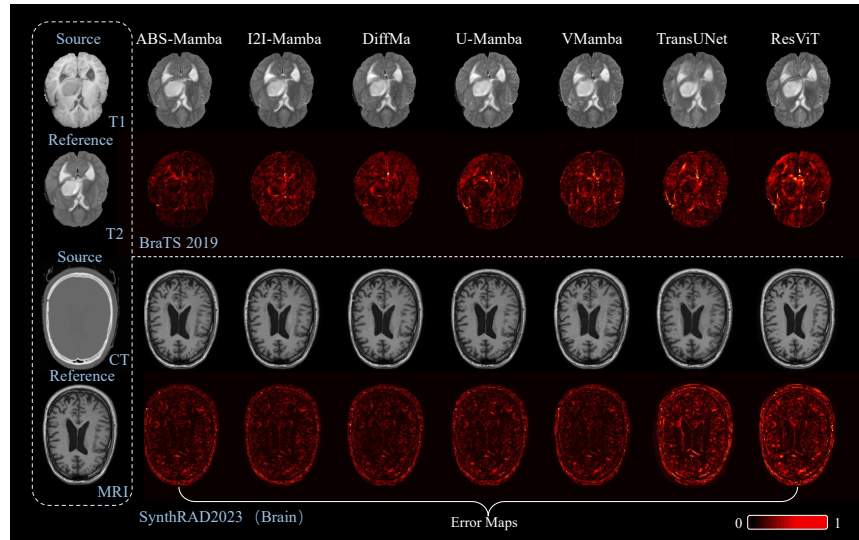


**Fig. 2.** Representative results for the T1 to T2 synthesis task on BraTS2019, show the source image, reference image, synthesized images by different methods, and difference maps between each synthesized image and the reference.

**Table 3.** Ablation studies of the different feature fusion strategies.

SIE	BRMN	RFFN	SSIM	SIE	BRMN	RFFN	SSIM
0	1	0	0.867	1	2	0	0.928
1	1	0	0.917	1	2	1	<b>0.935</b>
1	1	1	0.926	1	3	0	0.923
0	2	0	0.884	1	3	1	<u>0.931</u>

### 3.3 Ablation Studies

To investigate the effectiveness of the proposed modules, we conduct an ablation study on the BraTS2019 dataset. We evaluate the impact of incorporating the SAM2 Image Encoder (SIE) and RFFN, as well as varying numbers of BRMN modules, on image translation performance. The results are summarized in Table 3. The best performance is achieved when simultaneously incorporating the SIE and RFFN modules alongside BRMN, with the default configuration of 2 BRMN modules demonstrating a mean SSIM of 0.934. These results validate the effectiveness of fusing global semantic representations from the SAM2 encoder, localized detail features of medical images extracted by the CNNs encoder, and the efficient sequential bidirectional interaction mechanism of Mamba to achieve joint optimization for complementary cross-modal feature computation.

## 4 Conclusion

In this paper, we present ABS-Mamba, a novel medical image translation framework that synergistically integrates the global anatomical priors of SAM2 vision foundation models with Mamba’s efficient state space modeling. The architectural innovation is achieved through three key components: 1) a dual-stream encoder combining SAM2-Hiera’s anatomical prior preservation with CNNs-based local feature extraction. 2) spiral-scanned bidirectional Mamba blocks enabling linear-complexity modeling of multi-scale contextual dependencies. 3) hierarchical skip-connections with uncertainty-aware fusion for precise high-frequency detail reconstruction. The experimental validation conduct on multi-center brain and pelvic datasets demonstrates that ABS-Mamba offers precise anatomical accuracy in synthesizing high-quality target images. This innovation has potential to transform patient care by reducing the need for multiple imaging procedures, which minimizes radiation exposure and lowers healthcare costs. This advancement enhances patient safety and improves resource allocation efficiency.

## References

1. B. J. Pichler, M. S. Judenhofer, and C. Pfannenberger, *Multimodal Imaging Approaches: PET/CT and PET/MRI*. Springer, 2008, pp. 109-132.
2. L. Shen et al., “Multi-domain image completion for random missing input data,” *IEEE transactions on medical imaging*, vol. 40, no. 4, pp. 1113-1122, 2020.
3. B. Thukral, “Problems and preferences in pediatric imaging,” *Indian J. Radiol. Imaging*, vol. 25, pp. 359-364, 2015.
4. M. Havaei, N. Guizard, N. Chapados, and Y. Bengio, “HeMIS: Hetero-modal image segmentation,” in *Medical Image Computing and Computer-Assisted Intervention—MICCAI*. Cham, Switzerland: Springer, 2016, pp. 469-477.
5. T. Varsavsky, Z. Eaton-Rosen, C. H. Sudre, P. Nachev, and M. J. Cardoso, “PIMMS: Permutation invariant multi-modal segmentation,” in *Deep Learning in Medical Image Analysis and Multimodal Learning for Clinical Decision Support*. Cham, Switzerland: Springer, 2018, pp. 201-209.
6. A. Chatsias, T. Joyce, M. V. Giuffrida, and S. A. Tsiftaris, “Multimodal MR synthesis via modality-invariant latent representation,” *IEEE Trans. Med. Imag.*, vol. 37, no. 3, pp. 803-814, Mar. 2018.
7. Jeffrey D Rudie, Andreas M Rauschecker, R Nick Bryan, Christos Davatzikos, and Suyash Mohan. Emerging applications of artificial intelligence in neuro-oncology. *Radiology*, 290(3):607-618, 2019.
8. S. Roy, A. Carass, N. Shiee, D. L. Pham, and J. L. Prince, “Mr contrast synthesis for lesion segmentation,” in *2010 IEEE International Symposium on Biomedical Imaging: From Nano to Macro*. IEEE, 2010, pp. 932-935.
9. A. Adam, A. Dixon, J. Gillard, C. Schaefer-Prokop, R. Grainger, and D. Allison, *Grainger & Allison’s Diagnostic Radiology*. Elsevier, 2014.
10. Ming Li, Jiping Wang, Yang Chen, Yufei Tang, Zhongyi Wu, Yujin Qi, Haochuan Jiang, Jian Zheng, Benjamin M W Tsui. Low-dose CT Image Synthesis for Domain Adaptation Imaging Using a Generative Adversarial Network with Noise Encoding Transfer Learning[J]. *IEEE transactions on medical imaging*, Vol.42(9): 1, 2023

11. J. Chen, Y. Lu, Q. Yu, X. Luo, E. Adeli, Y. Wang et al., "TransUNet: Transformers make strong encoders for medical image segmentation," arXiv:2102.04306, 2021.
12. M. Heidari, S. G. Kolahi, S. Karimijafarbigloo, B. Azad, A. Bozorgpour, S. Hatami et al., "Computation-efficient era: A comprehensive survey of state space models in medical image analysis," arXiv:2406.03430, 2024.
13. J. Ma, F. Li, and B. Wang, "U-mamba: Enhancing long-range dependency for biomedical image segmentation," arXiv:2401.04722, 2024.
14. Z. Xing, T. Ye, Y. Yang, G. Liu, and L. Zhu, "Segmamba: Long-range sequential modeling mamba for 3d medical image segmentation," arXiv:2401.13560, 2024.
15. J. Liu, H. Yang, H.-Y. Zhou, Y. Xi, L. Yu, Y. Yu et al., "Swin-umamba: Mamba-based unet with imagenet-based pretraining," arXiv:2402.03302, 2024.
16. J. Huang, L. Yang, F. Wang, Y. Nan, A. I. Aviles-Rivero, C.-B. Sch"onlieb et al., "MambaMIR: An Arbitrary-Masked Mamba for Joint Medical Image Reconstruction and Uncertainty Estimation," arXiv:2402.18451, 2024.
17. Y. Yue and Z. Li, "Medmamba: Vision mamba for medical image classification," arXiv:2403.03849, 2024.
18. Alexander Kirillov, Eric Mintun, Nikhila Ravi, Hanzi Mao, Chloe Rolland, Laura Gustafson, Tete Xiao, Spencer Whitehead, Alexander C Berg, Wan-Yen Lo, et al., "Segment anything," in Proceedings of the IEEE/CVF International Conference on Computer Vision, 2023, pp. 4015-4026.
19. Nikhila Ravi, Valentin Gabeur, Yuan-Ting Hu, Ronghang Hu, Chaitanya Ryali, Tengyu Ma, Roman R"adle, Chloe Rolland, Laura Gustafson, et al., "Sam 2: Segment anything in images and videos," arXivpreprint arXiv:2408.00714, 2024.
20. Alexander Kirillov, Eric Mintun, Nikhila Ravi, Hanzi Mao, Chloe Rolland, Laura Gustafson, Tete Xiao, Spencer Whitehead, Alexander C. Berg, Wan-Yen Lo, Piotr Dollar, and Ross Girshick. Segment anything. In Proceedings of the IEEE/CVF International Conference on Computer Vision (ICCV), pages 4015-4026, October 2023.
21. Hayou, S., et al. (2024). LoRA+: Efficient Low Rank Adaptation of Large Models. arXiv preprint arXiv:2402.12354, 2024
22. Hu, Edward J. and Shen, Yelong and Wallis, Phillip and Allen-Zhu, Zeyuan and Li, Yuanzhi and Wang, Shean and Wang, Lu and Chen, Weizhu. LoRA: Low-Rank Adaptation of Large Language Models, arXiv:2106.09685, 2021.
23. Lin T Y, et al. Feature Pyramid Networks for Object Detection. CVPR 2017.
24. Ryali, C., Hu, Y.T., Bolya, D., Wei, C., Fan, H., Huang, P.Y., Aggarwal, V., Chowdhury, A., Poursaeed, O., Hoffman, J., et al.: Hiera: A hierarchical vision transformer without the bells-and-whistles. In: ICML. pp. 29441-29454. PMLR(2023)
25. Adrian Thummerer, Erik van der Bijl, Arthur Galapon Jr, Joost J C Verhoeff, Johannes A Langendijk, Stefan Both, Cornelis Nico A T van den Berg, Matteo Maspero. SynthRAD2023 Grand Challenge dataset: Generating synthetic CT for radiotherapy[J]. Medical physics, 2023, Vol.50(7): 4664-4674
26. Bakas, S. Brats MICCAI Brain tumor dataset. IEEE Dataport, 2020
27. O. Dalmaz, M. Yurt, and T. C.ukur, "ResViT: Residual vision transformers for multi-modal medical image synthesis," IEEE Trans Med Imaging, vol. 44, no. 10, pp. 2598-2614, 2022.
28. Liu, Y.; Tian, Y.; Zhao, Y.; Yu, H.; Xie, L.; Wang, Y.; Ye, Q.; and Liu, Y. 2024. Vmamba: Visual state space model. arXiv preprint arXiv:2401.10166.
29. J. Chen, Y. Lu, Q. Yu, X. Luo, E. Adeli, Y. Wang et al., "TransUNet: Transformers make strong encoders for medical image segmentation," arXiv:2102.04306, 2021.

30. Wang, Zhenbin and Zhang, Lei and Wang, Lituan and Zhang, Zhenwei. Soft Masked Mamba Diffusion Model for CT to MRI Conversion. arXiv preprint arXiv:2406.15910,2024
31. Omer F. Atli and Bilal Kabas and Fuat Arslan and Mahmut Yurt and Onat Dalmaz and Tolga Çukur. I2I-Mamba: Multi-modal medical image synthesis via selective state space modeling arXiv:2405.14022, 2024
32. Ma, J.; Li, F.; and Wang, B. 2024. U-mamba: Enhancing long-range dependency for biomedical image segmentation. arXiv:2401.04722.